scientific reports

Check for updates

OPEN

Therapeutic potential of targeting ceramide for early cardiometabolic lipotoxicity in vivo study

Youssef M. Shalaby[1], Bashar Al-Zohily[1], Manjusha Sudhadev[2], Abderrahim Nemmar[3], Suhail Al-Salam[2,4] & Nadia Akawi[1,5]✉

Ceramides (Cer) drive cardiometabolic disease (CMD) by promoting lipotoxicity and oxidative stress, yet their therapeutic potential remains underexplored. We investigated Cer dysregulation in high-fat diet (HFD) fed rats and evaluated three antidiabetic drugs (Sitagliptin, Liraglutide, Saxagliptin) for Cer-modulating effects. HFD elevated CerC16:0 and CerC18:0 across different tissues (serum, heart and liver), with pronounced cardiac CerC18:0 accumulation (1.37 ± 0.103 nmol/g, $p < 0.001$). Cer changes preceded alterations in traditional metabolic markers (glucose, cholesterol and triglycerides), suggesting early biomarker potential. In a five weeks pilot study ($n = 24$), Sitagliptin (Sita) outperformed Liraglutide and Saxagliptin in reducing Cer levels. Extended experiments ($n = 48$) showed Sita significantly decreased harmful Cer ratios (CerC16:0/24:0, CerC18:0/24:0), reduced oxidative stress and tissue lipid accumulation, while enhancing urinary CerC16:0 excretion index ($p < 0.01$). Sita restored cardioprotective signaling (eNOS, pAKT, cTnT) and mitigated apoptosis and steatosis. These findings highlight Cer as early indicators of lipotoxic injury and support Sita's potential for CMD therapy through modulation of Cer metabolism, warranting further clinical exploration.

Keywords Ceramide, Metabolic biomarkers, Cardiometabolic lipotoxicity, Oxidative stress, Sitagliptin

Ceramides (Cer) are lipid derivatives that are known to play a significant role in the pathogenesis of Cardiometabolic diseases (CMD)[1]. They have been shown to promote inflammation, apoptosis, oxidative stress, and insulin resistance, all of which are risk factors for cardiovascular diseases (CVD)[2,3]. One proposed mechanism for the role of Cer in CVD is through their effects on the endothelium, which is the inner lining of blood vessels[4]. Cer can impair endothelial function by promoting the production of reactive oxygen species (ROS), inducing inflammation, and inhibiting nitric oxide production. These effects can lead to endothelial dysfunction, which is a hallmark of CVD and characterized by impaired endothelial function, which can lead to atherosclerosis and other vascular disorders[1,5]. Moreover, major adverse cardiovascular events have been reported with higher plasma levels of CerC16:0, CeC18:0, and CerC24:1 but not with CerC22:0 and CerC24:0 in large human cohorts; however, further research is still needed to explore the exact mechanism by which Cer are involved in heart disease[6]. Recent studies highlight that Cer ratios, particularly CerC16:0/24:0, CerC18:0/24:0, and CerC24:1/24:0, are robust predictors of cardiometabolic risk and cardiovascular outcomes[7]. These ratios reflect an imbalance between pro-apoptotic, pro-inflammatory Cers (C16:0, C18:0) and their ratio to CerC24:0. Clinically, elevated CerC18:0/24:0 and CerC16:0/24:0 ratios associated with poor heart function and major cardiac events, independent of traditional risk factors[8]. Among them, the CerC24:1/24:0 ratio shows particular consistency across studies as a predictor of coronary heart disease risk[9]. Mechanistically, these ratios may reflect vascular endothelial dysfunction mediated by Cer-induced oxidative stress[10].

In animal models, high levels of total tissue Cer have been associated with metabolic and CVDs. It has been reported that genetic and pharmacological approaches to reduce total plasma Cer could reverse diet and glucocorticoid-induced insulin resistance, atherosclerosis, and metabolic cardiomyopathy in rodents[11–13]. More recent studies point toward the possibility that the adverse cardiometabolic effects of Cer could be more attributed to the remodeling of certain types (e.g., CerC16:0, CerC22:0, CerC24:0) than to total Cer levels[14,15].

[1]Department of Genetics and Genomics, College of Medicine and Health Sciences, United Arab Emirates University, Al Ain, UAE. [2]Department of Pathology, College of Medicine and Health Sciences, United Arab Emirates University, Al Ain, UAE. [3]Department of Physiology, College of Medicine and Health Sciences, United Arab Emirates University, Al Ain, UAE. [4]Zayed Center for Health Sciences, United Arab Emirates University, Al Ain, UAE. [5]Division of Cardiovascular Medicine, Radcliffe Department of Medicine, University of Oxford, Oxford, UK. ✉email: nadia.akawi@uaeu.ac.ae

Recent studies have highlighted that the balance between these Cer species is crucial for maintaining cellular homeostasis, with shifts in this balance contributing to metabolic disorders[16,17].

The current therapeutic approaches to CMD involve SGLT-2i, which inhibits glucose reabsorption from the kidney and GLP-1 receptor agonists that stimulate insulin secretion, reduce glucagon release and delay the gastric emptying time[18]. These drugs have demonstrated significant cardioprotective benefits, such as reducing the risk of major cardiovascular events and hospitalization due to heart failure and lowering cardiovascular and all-cause mortality[19]. Beyond glycemic control, SGLT-2i have been shown to modulate Cer metabolism and aging-related biomarkers, suggesting additional pathways for their cardiometabolic benefits[20]. Remarkably, Liraglutide (Lira), GLP-1 R agonist, +/- dapagliflozin (SGLT-2i) have shown significant cardioprotective impacts in diabetic rats that suffered from cardiomyopathy[21]. One proposed mechanism for these drugs' cardioprotective effects is their ability to reduce endothelial dysfunction[22]. For instance, Lira, Sitagliptin (Sita) and Empagliflozin have shown an improvement in endothelial function by reducing oxidative stress that occurs when there is an imbalance between the production of free radicals and the ability of the body to detoxify and repair the damage caused by these ROS[23,24].

This study investigates the effects of different antidiabetic medications on Cer metabolism in a high-fat diet (HFD) induced early stage of lipotoxicity in rat model. We aim to elucidate the mechanisms by which the best promising drug modulates Cer profiles, reduces oxidative stress, and improves cardiovascular and hepatic outcomes, providing insights into its therapeutic potential for early metabolic lipotoxicity.

Materials and methods

Animals

Seventy-two adult male Wistar rats weighing 200 ± 30 g were obtained from the animal house at the College of Medicine, United Arab Emirates University, UAE. The rats were housed under standard conditions: a 12-hour light/dark cycle, free access to standard rodent chow and water, a constant temperature of 25 ± 2 °C, and humidity of 60–70%. The animals have been acclimatized to laboratory conditions for two weeks prior to the experiment. Rats were housed 3–4 rats per cage with ad libitum access to regular chow or HFD of 60 kcal% fat (Cat# D12492, Research Diets, Inc, USA) and water. Animal treatments adhered strictly to international and institutional ethical guidelines (Directive 2010/63/EU) concerning the care and use of laboratory animals, with all experimental protocols approved by the United Arab Emirates University, College of Medicine and Health Sciences Committee for laboratory animal care in research (ethical approval No. ERA_2023_2491). Efforts were made to minimize animal suffering and reduce the number of animals used. This research adheres to the standards outlined in the ARRIVE guidelines for reporting animal experiments.

Experimental design

This research was conducted in two parts: a preliminary Pilot Study to screen potential therapeutic agents and a subsequent in-depth study on the most promising agent, Sitagliptin. Pilot Study: The primary aim of the pilot experiment was to assess the effects of Liraglutide (Lira; SML3925, Sigma), Sitagliptin (Sita; PHR1857, Sigma), and Saxagliptin (Saxa; Cat#945667, Sigma) on circulating Cer levels and their influence on the cardiovascular system in a rat model. Twenty-four Wistar rats (170–200 g) were randomly divided into four groups (n = 6 per group), as shown in Fig. S1A: Disease Control group received a high-fat diet (HFD) throughout the Pilot experiment. Lira group received HFD for 21 days, followed by Lira co-treatment (0.4 mg/kg/day s.c.) in normal saline (0.9%) for 14 days[25]. Sita group received HFD for 21 days, followed by co-treatment of Sita (5 mg/kg/day p.o.) in distilled water for 14 days[26]. Saxa group received HFD for 21 days, followed by Saxa co-administration (1 mg/kg/day p.o.) in distilled water for 14 days[27]. All animals were maintained on a normal chow diet prior to Day 0 to establish a within-group baseline, at which point the first blood sample was collected. On day 0, blood samples were collected to measure baseline blood glucose levels. Then, serum was separated for total cholesterol and Cer level measurements using the Trister Multi-Check Monitoring System (TS 391MC) and Tandem Mass Spectrometry, respectively. Subsequent blood samples were collected biweekly and Cer levels at all time points were compared to the Day 0 baseline within each group to assess longitudinal changes. Treatment began on day 22 and continued until day 35.

Following the Pilot Study, Sitagliptin Study was conducted: forty-eight Wistar rats (200–230 g) were divided into six groups as outlined in Fig. 1A (n = 8 per group) and two sequential experiments as follows: a short-term study (4 weeks), including groups I-III, with Cer measurements in serum at days 0, 14, and 28; and an extended experiment (12 weeks) in which blood and urine were collected from groups IV-VI at days 0, 60, and 90 for Cer and metabolic measurements, before termination at day 90. In Phase I, Group I (Negative Control; NC) had free access to standard rodent chow throughout the experiment. Group II (HFD Group): received HFD throughout the experiment. Group III (Sita Group): received HFD for 14 days, followed by Sita treatment (5 mg/kg) for the remaining period. While in the extended study (Phase II), Group IV (NC) had standard rodent chow throughout the experiment. Group V (HFD Group) received HFD throughout the experiment, and Group VI (Sita Group) received HFD for 60 days, followed by Sita treatment (5 mg/kg) for the final four weeks. On day 0, baseline glucose levels were measured from tail blood, and the serum was separated and stored at −80 °C for Cer analysis. At the end of the short-term phase, animals in Groups I, II, and III were euthanized on day 28, while animals in Groups IV, V, and VI were euthanized on day 90 at the end of the extended phase. Hearts and livers were isolated immediately post-euthanasia. Euthanasia was achieved by inducing deep anesthesia, monitored by lack of pedal reflex, with Pentobarbital ([90 mg/kg, IP], P3761, Sigma, USA), after which heart extraction was performed leading to exsanguination. Hearts (ventricular) and livers were either snap-frozen in liquid nitrogen for protein analysis, or specimens from each group were excised, washed in ice-cold saline, blotted with filter paper and then fixed in 10% formalin to be prepared for histopathological examination.

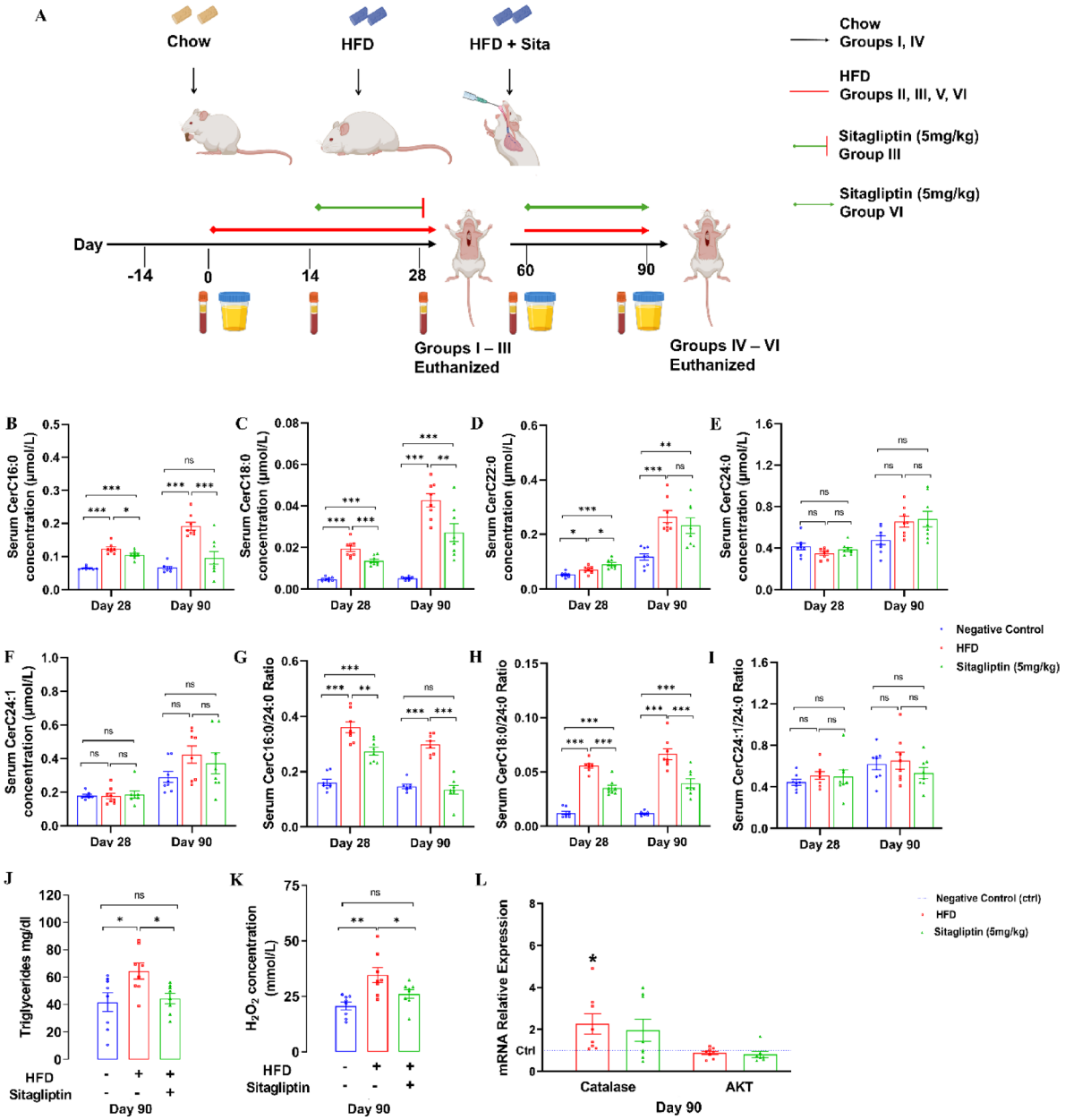

Fig. 1. Sitagliptin Modulates Serum Cer Profile, Oxidative Stress, and Catalase Gene Expression. (**A**) Schematic representation of the extended experimental design. Rats were fed either chow or a high-fat diet (HFD), followed by Sitagliptin treatment (5 mg/kg/day) at the indicated time points. Blood and urine samples were collected at 0, 60 and 90 time points, and animals were euthanized on days 28 and 90. (**B**-**D**) Serum concentrations of CerC16:0, CerC18:0, and CerC22:0 on days 28 and 90 in negative control (NC), high-fat diet (HFD), and Sitagliptin-treated groups. (**E**-**F**) Serum concentrations of CerC24:0 and CerC24:1. (**G**-**I**) Ratios of CerC16:0/24:0, CerC18:0/24:0, and CerC24:1/24:0 across the different groups. (**J**) Serum triglyceride (Day 90). (**K**) Serum H_2O_2 concentrations. Levels on Day 90. (**L**) Relative mRNA expression of each gene was normalized to GAPDH and represented relative to the expression of the normal diet group (dashed line). Data are presented as Mean ± SEM ($n = 8$ rats per group, biological replicates). Statistical analysis was performed using one-way ANOVA with Tukey's post hoc test (B–K) and unpaired Student's t-test (L). $^{*}p < 0.05$, $^{**}p < 0.01$, $^{***}p < 0.001$ indicates significance vs. Negative Control or HFD as indicated, ns = non-significant.

RNA purification and gene expression

Total RNA was extracted using QIAzol Lysis reagent (Cat#79306, Qiagen, Germany), followed by chloroform phase separation. RNA purity and concentration were assessed using a NanoDrop spectrophotometer (A260/280 = 1.9–2.1; A260/230 > 1.8). RNA integrity was confirmed by 1% agarose gel electrophoresis, visualizing clear 28 S and 18 S rRNA bands. cDNA synthesis was performed with the GoScript™ Reverse Transcriptase Kit (Cat# A5001, Promega, USA). Gene expression was quantified using SYBR™ Green Universal Master Mix (Cat#

4364344, Thermo Fisher, USA) on a QuantStudio™ 7 Flex Real-Time PCR System. GAPDH was used as the reference gene, and relative expression levels were calculated using the 2^(-ΔΔCt) method. Primers that were used are listed in Table S1.

Protein purification and western blot analysis

Heart tissues were homogenized in 10% (w/v) Radioimmunoprecipitation Assay (RIPA) buffer (Thermo Fisher 89901) containing 1% protease and phosphatase inhibitors (Thermo Scientific™ 78441). Protein concentration was determined using the BCA assay (Pierce™ BCA Protein Assay Kit, Cat#: 23225). A total of 20 µg of protein extract was loaded onto a 12% SDS-PAGE gel and transferred onto nitrocellulose membranes. The membranes were incubated overnight at 4 °C with primary antibodies: cTnT (1:1000, ab10214, Abcam), Akt (2:1000, 610860, BD Biosciences), pAkt (Ser473) (2:1000, 9271, Cell Signaling Technology), Caspase3/p17/p19 (2:1000, 66470-2-IG, Proteintech) and GAPDH (1:1000, PLA0125, Sigma). This was followed by a 1-hour incubation at room temperature with secondary antibodies: HRP-conjugated anti-rabbit (1:15000, A9169, Sigma) and HRP-conjugated anti-mouse (1:15000, A9044, Sigma). Protein bands were visualized using Azure Sapphire™ Biomolecular Imager via an enhanced chemiluminescence (Pierce™ ECL Plus Western Blotting Substrate Cat# 32132) detection system, and pixel density and area were assessed using ImageJ software. Density readings were normalized to GAPDH signal intensity.

Urinalysis

Twenty-four-hour urine was collected in metabolic cages on days 0, 60 and 90. Urine creatinine and albumin were measured using a Cobas C111 Chemistry Analyzer (Roche Diagnostics). Creatinine was determined using an enzymatic colorimetric assay, and albumin was measured via an immunoturbidimetric method. All procedures were performed according to the manufacturer's instructions. The urine albumin: creatinine ratio (UACR) was calculated in mg/g to evaluate albuminuria.

Lipidomics

Briefly, 100 mg of frozen myocardial tissue was homogenized in phosphate-buffered saline (PBS) at pH 7.4 using an electric homogenizer (ULTRA-TURRAX® T 25 basic IKA®, Germany). Following the thawing of rat serum/urine samples, which were previously frozen and stored at −80℃, they were subjected to vortexing, and then 250 µl of each sample was transferred into a new glass tube to initiate a liquid-liquid extraction process. After that, 50 µl of a mixture of CerC16:0-d7, CerC18:0-d7, CerC24:0-d7, and CerC24:1-d7, which acted as internal standard, was added to the samples. To extract the Cer metabolites and their internal standards from the samples, 1 ml of a mixture of hexane and ethyl acetate (9:1) was added; afterwards, the resulting solution was subjected to vortexing for a few minutes. Then, the mixture underwent centrifugation at a speed of 4000 rpm for a duration of 15 min at room temperature. The supernatant layer was isolated and transferred to a new test tube, and an additional extraction was conducted on the remaining lower layer. All the extracted layers were pooled together and dried at room temperature using a gentle stream of nitrogen gas in a sample concentrator. Finally, 100 ul of a mixture of water, acetonitrile, and isopropanol (5%: 47.5%: 47.5%) of LC-MS/MS grade was added to reconstitute the residue.

Cytokine quantification

Levels of TNF-α and IL-6 were quantified from the cleared protein lysates previously prepared for Western blot analysis. We used commercial rat sandwich ELISA kits (TNF-α, Cat# DY510; IL-6, Cat# DY506; R&D Systems, Minneapolis, USA) according to the manufacturer's instructions. Cytokine concentrations were determined from a standard curve and normalized to the total protein concentration of each sample. Results are expressed as pg of cytokine per mg of total protein.

Triglycerides assay

Triglyceride levels were measured using the Triglyceride Quantification Assay Kit according to the manufacturer's instructions (Cat# ab65336). Samples and standards were prepared in duplicate, with triglycerides converted to glycerol and free fatty acids by adding lipase and incubating at room temperature for 20 min. A reaction mix containing assay buffer, probe, and enzyme was added to each well, followed by a 60-minute incubation at room temperature in the dark. Absorbance was measured at 570 nm (colorimetric). Sample readings were compared to a standard curve to determine triglyceride concentrations.

Ceramides assay by ultra high-pressure liquid chromatography-tandem mass spectrometry (uhplc-ms/ms) instrument

The instrument comprises of Waters Acquity UPLC® I class Plus system, paired with a Triple Quadrupole Mass Spectrometer [Xevo TQ-S micro (Waters, Milford, USA)]. The chromatography technique was applied to separate the Cer based on their molecular weights and polarities using an Acquity UPLC BEH (Ethylene Bridged Hybrid) C18 column (dimensions: 2.1 mm x 50 mm x 1.7 µm). To extend the lifespan of the analytical column, the C18 column was connected with the guard column for physical filtration. The injection volume of the sample was 2 µl. Before and after each injection, the needle was washed using a wash program in the system with water/acetonitrile (25:75, v/v) to minimize contamination and carryover. The mobile phase's flow rate and the column's temperature were set to 0.3 ml/min and 40℃, respectively. The gradient pump mode was operated for chromatographic separation by using two mobile phases, including mobile phase A (100% water + 10 mM ammonium formate + 0.1% formic acid) and mobile phase B (5% water/47.5% acetonitrile/47.5% isopropanol + 10 mM ammonium formate + 0.1% formic acid). The optimal mobile phase gradient for Cer separation started at 85% of mobile phase B from 0 to 0.5 min. Then, it was increased and maintained at 100%

from 0.51 to 4.0 min. After that, mobile phase A was increased to 25% while B decreased to 85% from 4.01 to 5.0 min for the equilibration step.

Under the applied Electrospray Ionization (ESI) source, the Multiple Reaction Monitoring (MRM) transitions for all Cer and their internal standards generate the protonated molecules, [M + H]+. The most abundant precursor ions of Cer and internal standards were detected after the loss of water molecule and the most sensitive fragment ion was observed at a mass-to-charge ratio (m/z) 264.3 for Cer and at m/z 271.3 for deuterated Cer (Internal Standard); therefore, the MRM transitions of CerC16:0, CerC18:0, CerC22:0, CerC24:0, CerC24:1, CerC16:0-d7, CerC18:0-d7, CerC24:0-d7, and CerC24:1-d7 were 520.6 > 264.3, 548.6 > 264.3, 604.6 > 264.3, 632.6 > 264.3, 630.6 > 264.3, 527.5 > 271.3, 555.6 > 271.3, 639.7 > 271.3, and 637.4 > 271.3; respectively. These MRM transitions were optimized by performing the direct infusion of each Cer standard into the mass spectrometer (Xevo TQ-S micro) system. The UHPLC-MS/MS parameters and data were managed and handled using the Masslynx software. The above method for qualitative and quantitative Cer in biological samples was previously optimized, developed and validated as described previously[28].

ROS measurement

The ROS levels in the rat serum were measured using a Hydrogen Peroxide (H_2O_2) Assay Kit (Elabscience, Cat# E-BC-K102-M, USA). Samples were detected directly without dilution, according to the kit's protocol. The procedure for detection was as follows: 100 µL buffer solution was added to the standard and sample wells. Then, the plate was preheated at 37 °C for 10 min. Later, 15 µL of the gradient standards and serum samples were added to their corresponding wells and mixed with 100 µL of ammonium molybdate reagent. Lastly, they were incubated for 10 min at room temperature, after which the absorbance was read on a microplate reader at 405 nm. The content of H_2O_2 was calculated by a standard curve developed with increasing concentrations of known H_2O_2.

Histopathological examination

Liver and heart were sliced, cassetted and fixed directly in 10% buffered formalin for 24 h, which was followed by dehydration in increasing concentrations of ethanol, clearing with xylene and embedding with paraffin. Three-micrometer sections were prepared from paraffin blocks and stained with hematoxylin and eosin stain using standard procedures. For each stained slide, five non-overlapping high-power fields (20x magnification) were examined to assess structural changes. Quantitative morphometric analysis of lipid accumulation was performed using ImageJ software on the stained sections. Images were converted to 8-bit, a uniform threshold was applied to identify clear cytoplasmic vacuoles characteristic of microvesicular lipid droplets, and the average number of droplets was then calculated.

Statistical analysis

The data obtained were analyzed through GraphPad Prism version 8.0 software (GraphPad Software, San Diego, CA, USA). Parametric data are presented as mean ± standard error of the mean (SEM) as they passed the normality test (Shapiro-Wilk test); for non-parametric data, they are given as Median (IQR). $p < 0.05$ was considered statistically significant. Where appropriate, a comparison between two points was made using either the Student's t-test or the Wilcoxon Matched-Pairs Signed Rank test. In contrast, one-way ANOVA or Kruskal-Wallis test was used to compare changes between the different groups over time, followed by Tukey's or Dunn's post hoc tests for multiple comparisons. All statistical analyses were based on biological replicates (individual animals). For molecular assays at least three technical replicates were performed per biological sample and the mean/median values were used for statistical comparisons.

Results

Evaluation of antidiabetic drug efficacy in modulating ceramide levels

Given the critical role of Cers in metabolic dysfunction, the Pilot Study (Fig. S1A) aimed to define the time course of HFD-induced Cer (C16:0, C18:0, C22:0, C24:0, C24:1) accumulation and subsequently assess the modulatory effects of glucose-lowering agents namely, Lira, Sita and Saxa on serum Cer levels. Similar trends were observed for CerC16:0 and CerC18:0, as both levels remained elevated over the 35-day study duration in the HFD and Lira groups (Figs. S1B and S1C). In the HFD group, CerC16:0 levels increased from a median of 0.094 µmol/L (IQR: 0.085–0.103) to 0.142 µmol/L (IQR: 0.11–0.18) within five weeks ($p < 0.05$), while CerC18:0 levels rose from 0.007 µmol/L (IQR: 0.006–0.0085) to 0.023 µmol/L (IQR: 0.018–0.026) ($p < 0.05$) during the same time. Similarly, in the Lira group, CerC16:0 levels increased from 0.13 µmol/L (IQR: 0.121–0.156) to 0.162 µmol/L (IQR: 0.137–0.191), and CerC18:0 levels rose from 0.0105 µmol/L (IQR: 0.0065–0.012) to 0.0244 µmol/L (IQR: 0.0192–0.0312) ($p < 0.05$ for both), indicating that Lira did not attenuate HFD-induced Cer accumulation. In contrast, Sita demonstrated significant reductions in Cer levels: CerC16:0 increased from 0.0985 µmol/L (IQR: 0.085–0.134) at day 0 to 0.14 µmol/L (IQR: 0.119–0.176) three weeks later then started to decrease significantly one week after the treatment, reaching 0.116 µmol/L (IQR: 0.0949–0.132) by day 35 ($p = 0.7842$ vs. day 0; Fig. S1B), while CerC18:0 doubled from 0.0125 µmol/L (IQR: 0.0113–0.0168) to 0.0268 µmol/L (IQR: 0.0179–0.0347) at day 21 but decreased significantly to 0.0169 µmol/L (IQR: 0.0139–0.0214) by day 35 ($p = 0.36$; Fig. S1C). Saxa showed partial efficacy, reducing CerC16:0 levels from 0.16 µmol/L (IQR: 0.15–0.206) at day 21 to 0.0836 µmol/L (IQR: 0.0673–0.103) by day 35 ($p = 0.46$ vs. day 0; Fig. S1B), but had no significant effect on CerC18:0 levels, which remained elevated at 0.0118 µmol/L (IQR: 0.0102–0.0147) compared to day 0 ($p < 0.05$; Fig. S1C). Body weight increased progressively in all the groups, with a significant difference observed between the Lira and HFD (Mean ± SEM) at day 35 (287 ± 7.9 g vs. 348 ± 13.4 g, $p < 0.01$; Fig. S1D) while fasting blood glucose (range: 68–177 mg/dl; Fig. S1E) and total cholesterol levels (range: 105–135 mg/dl; Fig. S1F) remained

stable across all groups ($p > 0.05$). These findings highlight Sita's superior efficacy in modulating Cer metabolism, with significant reductions in both CerC16:0 and CerC18:0 levels.

Sitagliptin modulates blood ceramide profile, normalizes metabolic biomarkers, and reduces oxidative stress

In the Sitagliptin Study (Fig. 1A), our objective was to explore Sita's therapeutic potential in modulating the circulating levels of Cer species across multiple time points to elucidate its broader cardioprotective mechanisms beyond glycemic control. At baseline (day 0), no significant differences in Cer levels were observed between the different groups, confirming that all groups were comparable before the intervention. By day 14, HFD feeding had already induced significant increases in serum levels of CerC16:0 (both groups: $p < 0.001$), CerC16:0/24:0 ratio (both groups: $p < 0.001$), CerC18:0 (Group II: $p < 0.001$; Group III: $p < 0.01$) and CerC18:0/24:0 ratio (both groups: $p < 0.001$) compared to the NC group (Group I). Notably, Group III exhibited a reduction in CerC24:1 level compared to the NC group, though these changes did not reach statistical significance relative to the HFD group (Group II) (Table S2). This trend may reflect inherent metabolic variability or early compensatory mechanisms preceding Sita intervention. Similarly, by day 60 of Phase II, prior to the initiation of Sita treatment, both the HFD (Group V) and Sita (Group VI) groups exhibited comparable and significant elevations in serum CerC16:0 ($p < 0.01$), CerC16:0/24:0 ratio ($p < 0.001$), CerC18:0 ($p < 0.001$), CerC18:0/24:0 ratio ($p < 0.001$) and CerC22:0 ($p < 0.05$) compared to the NC group (Group IV) (Table S3). Although a similar pattern of Cer alterations was observed in both experiments by the end of days 28 and 90, the effects were more pronounced at day 90 (Fig. 1B and I). HFD-fed rats exhibited a significant increases in CerC16:0 [0.192 ± 0.0118 vs. 0.0655 ± 0.0053 µmol/L ($p < 0.001$)]; CerC18:0 [0.0427 ± 0.0031 vs. 0.00525 ± 0.0003 µmol/L ($p < 0.001$)]; and CerC22:0 [0.266 ± 0.0221vs. 0.117 ± 0.0123 µmol/L ($p < 0.001$)] compared to the NC Group (Fig. 1B and D; Mean ± SEM). Sita treatment significantly reduced CerC16:0 [0.0958 ± 0.0196 µmol/L ($p < 0.001$)] and CerC18:0 [0.0271 ± 0.0043 µmol/L ($p < 0.01$)] levels in serum compared to the HFD group, while there was a non-significant decrease in CerC22:0 [0.232 ± 0.0282 µmol/L ($p > 0.05$)]. Paradoxically, CerC24:0 levels remained unchanged across all groups ($p > 0.05$): NC [0.476 ± 0.044 µmol/L], HFD [0.654 ± 0.0505 µmol/L], and Sita [0.680 ± 0.0752 µmol/L]. Similarly, CerC24:1 level did not differ significantly ($p > 0.05$): NC [0.289 ± 0.0328 µmol/L], HFD [0.423 ± 0.0511 µmol/L], and Sita [0.371 ± 0.0615 µmol/L] (Fig. 1E and F).

Additionally, significant elevations in CerC16:0/24:0 [0.298 ± 0.0130 vs. 0.147± 0.0077 ($p < 0.001$)] and CerC18:0/24:0 [0.0664 ± 0.005 vs. 0.0117± 0.0007 ($p < 0.001$)] ratios were observed in the HFD group, indicating a shift toward a more lipotoxic Cer profile compared to the controls. Sita treatment restored the CerC16:0/24:0 ratio to levels comparable to NC [0.134 ± 0.0156 vs. 0.147 ± 0.0077 ($p > 0.05$)] (Fig. 1G), while CerC18:0/24:0 was significantly reduced [0.0396 ± 0.00410 ($p < 0.001$)] but not fully normalized (Fig. 1H). CerC24:1/24:0 ratios did not differ significantly ($p > 0.05$): NC [0.622 ± 0.0552 µmol/L], HFD [0.654 ± 0.0798 µmol/L], and Sita [0.534 ± 0.0519 µmol/L] (Fig. 1I).

To determine whether Cer dysregulation coincided with changes in classical metabolic parameters, we evaluated serum levels of triglycerides, cholesterol, and fasting blood glucose. These markers are commonly associated with cardiometabolic risk and may provide further context for Cer-driven metabolic dysfunction. While all groups exhibited progressive weight gain (most notably in HFD-fed rats), only triglycerides showed significant alterations among metabolic markers at Day 90. Serum triglyceride levels were significantly elevated in the HFD groups compared to the NC group [64.4 ± 5.75 vs. 41.8 ± 6.82 mg/dl ($p < 0.05$)] and were effectively reduced by Sita [44.5 ± 3.69 mmol/L ($p < 0.05$)] (Fig. 1J). On the other hand, both cholesterol and fasting glucose remained within normal ranges across groups, with HFD rats showing Mean ± SEM values of 119.3 ± 4.566 mg/dl (Day 60) and 129.8 ± 2.808 mg/dl (Day 90) for cholesterol, and 123.5 ± 2.797 mg/dl (Day 60) and 133.6 ± 2.345 mg/dl (Day 90) for glucose, comparable to control levels (Table S4).

Since oxidative stress is a key contributor to Cer-induced metabolic dysfunction, we assessed ROS levels and found that serum H_2O_2 concentrations exhibited significantly higher levels in the HFD group versus the NC [34.5 ± 3.35 vs. 20.7 ± 1.73 mmol/L ($p < 0.01$)] on Day 90, which were reduced upon Sita treatment [26 ± 1.93 mmol/L ($p < 0.05$)] (Fig. 1K). Supporting this finding, RT-qPCR analysis revealed that catalase expression, a key antioxidant enzyme, was significantly upregulated in the HFD group compared to the NC ($p < 0.05$) but normalized following Sita treatment. In contrast, AKT expression (Day 90), despite its role in cell survival and metabolism, did not show significant alterations ($p > 0.05$) across groups (Fig. 1L), suggesting that Cer-induced effects may occur at the level of AKT phosphorylation rather than its gene expression.

Sitagliptin reduces cardiac ceramide levels, modulates the expression of key signaling proteins related to cardiac function and stress responses

To investigate the Cer accumulation in the rodents' hearts, we next examined their cardiac Cer content at days 28 and 90 by analyzing tissue samples obtained from the six groups of the Sitagliptin Study. Unlike serum, HFD feeding significantly elevated all cardiac Cer levels at the end of the study ($p < 0.01$), with a similar trend observed between day 28 and day 90. Specifically, significant increases were observed in CerC16:0 [0.879 ± 0.0553 vs. 0.269 ± 0.0289 nmol/g ($p < 0.001$)]; CerC18:0 [1.37 ± 0.103 vs. 0.274± 0.0319 nmol/g ($p < 0.001$)]; CerC22:0 [0.41 ± 0.0365 vs. 0.234± 0.0293 nmol/g ($p < 0.01$)]; CerC24:0 [0.308 ± 0.0115 vs. 0.212 ± 0.0156 nmol/g ($p < 0.001$)]; CerC24:1 [0.344 ± 0.0145 vs. 0.129 ± 0.0108 nmol/g ($p < 0.001$)] compared to the NC. Additionally, CerC16:0/24:0 [2.86 ± 0.137 vs. 1.26 ± 0.101 ($p < 0.001$)]; CerC18:0/24:0 [4.41 ± 0.235 vs. 1.28 ± 0.109 ($p < 0.001$)]; CerC24:1/24:0 [1.12 ± 0.0284 vs. 0.615 ±0.0424 ($p < 0.001$)] ratios were significantly elevated in the HFD group (Fig. 2A and H; Mean ± SEM).

Sita treatment mitigated the accumulation of cardiac Cer, significantly reducing levels of CerC16:0 [0.402 ± 0.0388 nmol/g ($p < 0.001$)]; CerC18:0 [0.660 ± 0.0653 nmol/g ($p < 0.001$)]; CerC22:0 [0.228 ± 0.0261 nmol/g ($p < 0.01$)]; CerC24:0 [0.204 ± 0.0162 nmol/g ($p < 0.001$)] and CerC24:1 [0.168 ± 0.0164 nmol/g ($p < 0.001$)];

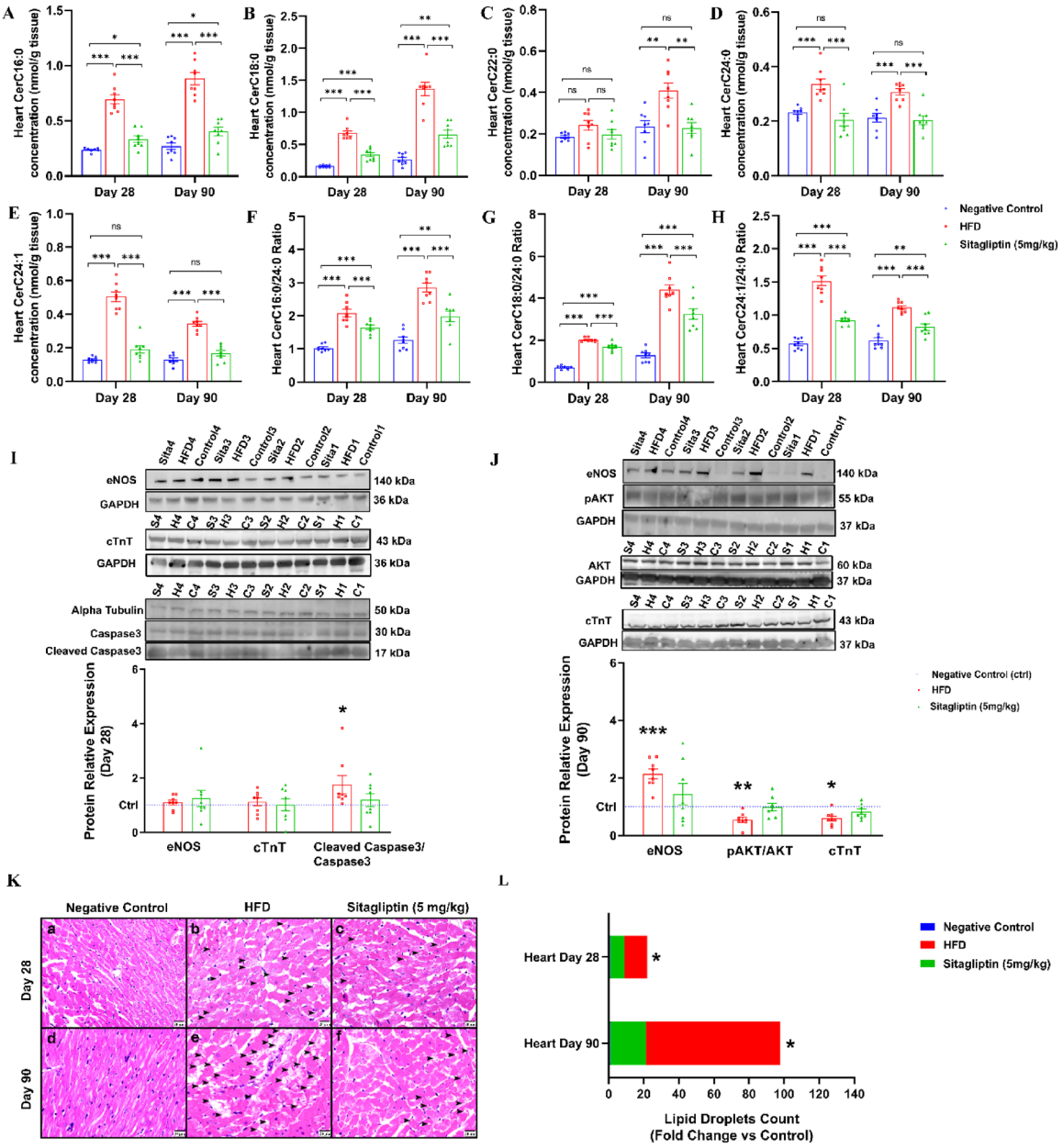

Fig. 2. Effects of Sitagliptin on Cardiac Cer Profile and Protein Expression. (**A**-**E**) Quantification of heart Cer species (CerC16:0, CerC18:0, CerC22:0, CerC24:0) at days 28 and 90. (**F**-**H**) Ratios of Cer species in heart tissues ($n = 8$ rats per group, biological replicates). (**I**) Representative Western blot images and quantification of eNOS, cTnT, and Cleaved Caspase-3 on day 28 ($n = 8$). (**J**) Protein expression of eNOS, pAKT and cTnT on day 90 ($n = 8$ rats per group, biological replicates). Relative protein expression was normalized to GAPDH, and the control group was on a normal diet (dashed line). (K_{a-c}) corresponds to day 28 and (K_{d-f}) to day 90, showing histological changes in H&E-stained heart sections ($n = 3$). Control groups (K_a, K_d) exhibit normal myocardial architecture. HFD groups (K_b, K_e) show marked lipid accumulation within cardiomyocytes (arrowheads). Sitagliptin-treated groups (K_c, K_f) demonstrate reduced intracellular fat globules and partial restoration of myocardial integrity. Scale bar: 20 µm. (**L**) Stacked bar chart representing the relative abundance of lipid droplets across groups. Statistical analysis was performed using one-way ANOVA with Tukey's post hoc test (A-J) and Kruskal-Wallis with Dunn's multiple comparisons test (L). Data are presented as Mean ± SEM. $^{*}p < 0.05$, $^{**}p < 0.01$, $^{***}p < 0.001$, ns = non-significant.

CerC16:0/24:0 ratio [1.98 ± 0.157 ($p < 0.001$)]; CerC18:0/24:0 [3.25 ± 0.257 ($p < 0.001$)]; CerC24:1/24:0 ratio [0.821 ± 0.0516 ($p < 0.001$)] (Fig. 2A and H; Mean ± SEM). These effects were more pronounced at day 90, suggesting a cumulative impact of prolonged Sita intervention.

Next, to reveal the effect of Cer and Sita on the cardiovascular disease-related pathological mechanisms, the key signaling proteins implicated in cardiac function and stress responses were investigated (Fig. 2I and J). On

day 28, HFD-fed rats exhibited a significant upregulation of Cleaved Caspase-3 expression ($p < 0.05$), indicative of increased apoptosis. At the same time, endothelial nitric acid synthase (eNOS) and cardiac troponin T (cTnT) levels remained unchanged. Sita treatment mitigated Cleaved Caspase-3 activation, suggesting a protective effect against HFD-induced cardiomyocyte apoptosis. By day 90, eNOS expression was significantly increased in the HFD group ($P < 0.001$) compared to the NC group, accompanied by a reduction in phosphorylated AKT (pAKT) and cTnT levels ($p < 0.05$ for both). Sita administration effectively restored eNOS and pAKT expression while preventing the decline in cTnT levels, indicating improved endothelial function and cardiomyocyte integrity. These findings highlight a persistent pattern of Cer dysregulation and oxidative stress under HFD conditions, with Sita exerting cardioprotective effects that became more evident over time.

Next, a histopathological examination of heart tissues was carried out to explore the morphological alterations in response to HFD feeding and Sita treatment. In the heart, both control groups (I and IV) showed normal myocardial architecture with intact cardiomyocytes and limited lipid accumulation (Figs. $2K_a$ and $2K_d$), while HFD groups exhibited intracellular lipid droplet accumulation in cardiomyocytes at days 28 (Fig. $2K_b$) and 90 (Fig. $2K_e$), indicative of lipotoxic injury. Sita treatment significantly reduced lipid droplet density (Figs. $2K_c$ and $2K_f$), correlating with improved Cer profiles and molecular markers. Figures 2L displays the quantified lipid droplets in each slide of heart sections.

Liver ceramide profile is altered by HFD and partially restored by sitagliptin over time

We next examined whether hepatic Cer concentrations were altered at days 28 and 90 in response to HFD feeding and Sita treatment. HFD significantly increased all the aforementioned Cer types compared to the NC at both time points ($p < 0.01$), with an even greater elevation observed at the later time points, emphasizing the progressive nature of Cer dysregulation under chronic HFD conditions. Remarkably, on day 90, hepatic CerC16:0 levels in the HFD group reached [1.44 ± 0.0453 nmol/g] compared to [0.221 ± 0.0222 nmol/g] in the NC group ($p < 0.001$). Similarly, CerC18:0 levels rose to [0.364 ± 0.0141 nmol/g] vs. [0.0388 ± 0.0042 nmol/g] ($p < 0.001$), and CerC22:0 levels increased to [1.37 ± 0.0467 nmol/g] vs. [0.217 ± 0.0226 nmol/g] ($p < 0.001$). The longer-chain Cers, CerC24:0 and CerC24:1, also showed significant elevations, with levels reaching [2.10 ± 0.0878 nmol/g] and [1.6 ± 0.128 nmol/g], respectively, compared to [0.684 ± 0.0558 nmol/g] and [0.321 ± 0.0265 nmol/g] in the NC group ($p < 0.001$ for both). A similar trend was observed on day 28, though the increases were less pronounced, highlighting the time-dependent exacerbation of Cer accumulation (Fig. 3A and E). Sita treatment attenuated this accumulation, significantly reducing hepatic levels of all Cer species compared to the HFD group at day 90 ($p < 0.001$ for all). Specifically, CerC16:0 levels decreased to [0.358 ± 0.0417 nmol/g], CerC18:0 to [0.148 ± 0.0219 nmol/g], CerC22:0 to [0.437 ± 0.0667 nmol/g], CerC24:0 to [0.895 ± 0.109 nmol/g], and CerC24:1 to [0.484 ± 0.0511 nmol/g]. Notably, HFD-induced elevations in CerC16:0/24:0, CerC18:0/24:0 and CerC24:1/24:0 ratios were evident as well [0.687 ± 0.0208 vs. 0.320 ± 0.0121 ($P < 0.001$)], [0.174 ± 0.0047 vs. 0.057 ± 0.0046 ($P < 0.001$)] and [0.754 ± 0.0430 vs. 0.472 ± 0.0136 ($P < 0.01$)], respectively, reflecting an imbalance in Cer metabolism. Sita significantly decreased CerC16:0/24:0 [0.409 ± 0.0239 ($p < 0.001$)] and CerC24:1/24:0 [0.559 ± 0.0346 ($p < 0.01$)] ratios, yet the CerC18:0/24:0 ratio remained elevated [0.162 ± 0.00640 ($p > 0.05$)] (Fig. 3F and H).

Histopathological analysis of liver sections revealed normal hepatic structure in the control group, with well-organized hepatocytes and no evidence of lipid accumulation (Figs. $3I_a$ and $3I_d$). In the HFD group, extensive hepatic microvesicular steatosis was evident, indicating significant lipid accumulation (Figs. $3I_b$ and $3I_e$). The degree of steatosis was more pronounced on day 90, suggesting progressive liver injury over time. Sita treatment led to a notable reduction in lipid droplets and the number of hepatocytes affected by steatosis compared to the HFD group (Figs. $3I_c$ and $3I_f$), paralleling its effect on hepatic Cers levels. Figure 3J displays the quantified lipid droplets in each slide of liver sections. To further investigate whether Cer accumulation was accompanied by inflammatory responses, levels of interleukin-6 (IL-6) and tumor necrosis factor-α (TNF-α) were quantified in liver homogenates (Fig. 3K and L). Both cytokines were significantly elevated in the HFD rats compared to the NC group ($p < 0.05$), indicating activation of pro-inflammatory signaling pathways under metabolic stress. Sita treatment markedly reduced the mean levels of IL-6 and TNF-compared to the HFD group, approaching control values, although these reductions did not reach statistical significance.

Urinary ceramide excretion and renal function in experimental groups

To identify potential elimination pathways contributing to the observed reductions in circulating and tissue Cer levels, we collected 24-hour urine output on days 0, 60 and 90 and noticed a significant reduction in urine volume in Groups V and VI on day 60 compared to the NC group ($P < 0.001$; Table S5). By the end of the experiment, urine output remained persistently lower in the HFD rats (Group V) relative to the other two groups (Fig. 4A and B), provoking an assessment of renal function. In consistent with the reduced urine volume, urine creatinine concentration was significantly higher in the HFD group than in the NC group ($p < 0.05$, Fig. 4C). However, the urine albumin and albumin-to-creatinine ratio (UACR), a key indicator of renal damage, were not significantly different among any of the experimental groups ($p > 0.05$ Fig. 4D and E). This suggests that while the high-fat diet altered fluid balance and urine concentration, it did not induce significant albuminuria by day 90.

Having established that overt renal injury was not a confounding factor, we next investigated whether Cer reduction is reflected in urinary excretion and assessed the urinary excretion index of CerC16:0, CerC18:0, CerC22:0, CerC24:0, and CerC24:1 on day 90. Interestingly, the urinary excretion index of CerC16:0 was significantly increased in the Sita-treated group compared to both the NC ($p < 0.01$) and HFD ($p < 0.05$) groups (Fig. 4F). However, no significant difference was observed between the HFD and NC groups, suggesting that Sita specifically enhances the excretion of CerC16:0. For CerC18:0, the excretion index was significantly reduced in the HFD group compared to the NC ($p < 0.05$), but Sita did not alter substantially this parameter (Fig. 4G). The

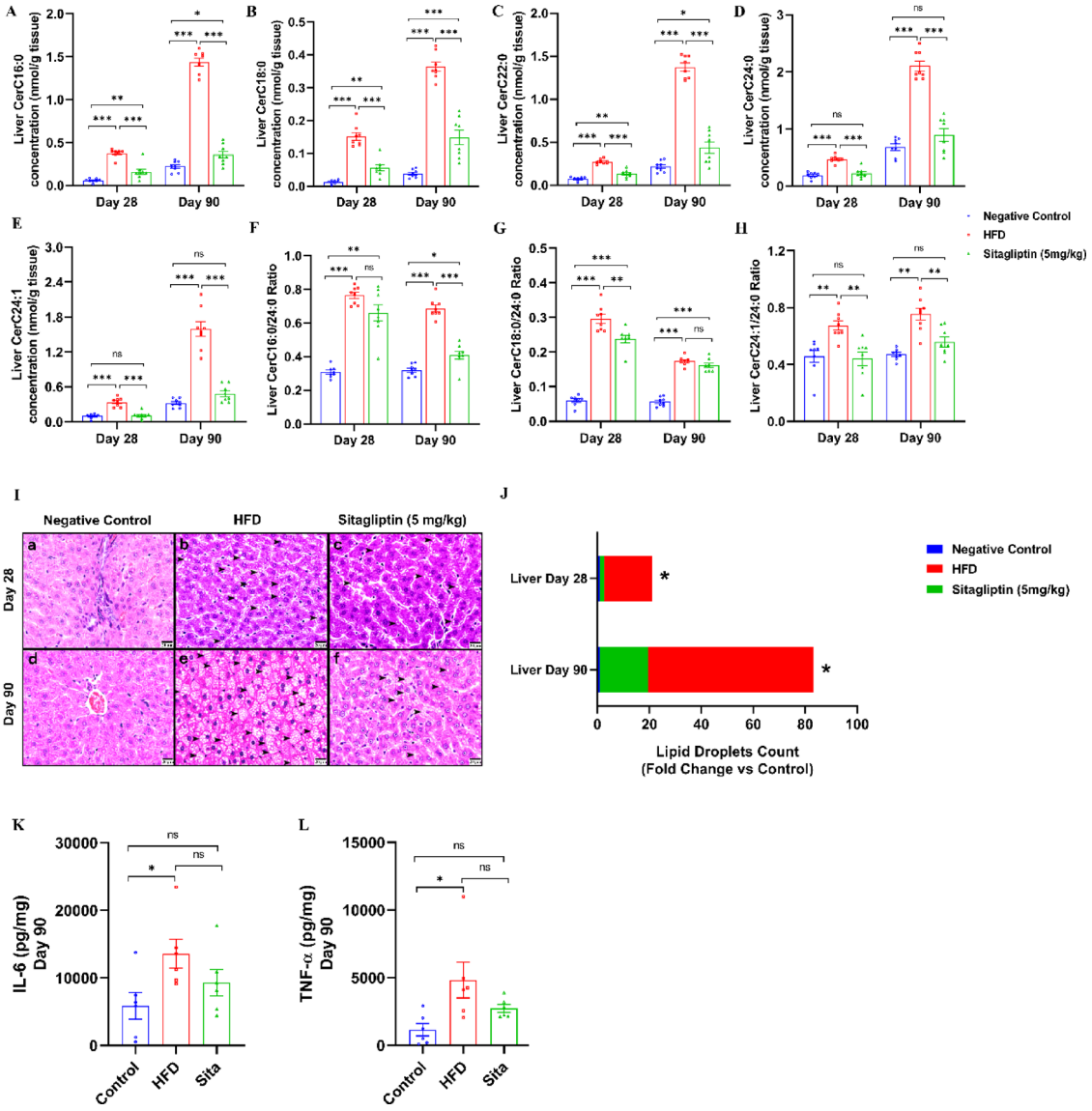

Fig. 3. Sitagliptin Modulates Liver Lipids Profile Including High-Risk Cers and Inflammatory Cytokines. (**A**-**E**) Quantification of liver Cer species (CerC16:0, CerC18:0, CerC22:0, CerC24:0) at days 28 and day 90. (**F**-**H**) Ratios of Cer species in liver tissues ($n = 8$ rats per group). (I_{a-c}) corresponds to day 28 and (I_{d-f}) to day 90, showing histological changes in H&E-stained liver sections ($n = 3$). Control groups (I_a, I_d) exhibit normal liver histology. HFD groups (I_b, I_e) show widespread microvesicular steatosis, with numerous hepatocytes containing lipid vacuoles (arrowheads). Sitagliptin-treated groups (I_c, I_f) display a reduction in lipid accumulation and restoration of the hepatic structure. Scale bar: 20 µm. (**K**) Hepatic IL-6 and (**L**) TNF-α levels, demonstrating significant elevations in the HFD group versus the control group. Statistical analysis was performed using one-way ANOVA with Tukey's post hoc test (A-H, K, L) and Kruskal-Wallis with Dunn's multiple comparisons test (**J**). Data are presented as Mean ± SEM. $^*p < 0.05$, $^{**}p < 0.01$, $^{***}p < 0.001$, ns = non-significant.

urinary excretion indices of CerC22:0, CerC24:0, and CerC24:1 remained unchanged across all groups (Fig. 4H and I).

Discussion

This study provides insights into the therapeutic potential of targeting Cer metabolism for early lipotoxcity, demonstrating that Sita, a dipeptidyl peptidase 4 (DPP-4) inhibitor, outperforms Lira and Saxa in modulating Cer profiles, attenuating oxidative stress, and improving cardiovascular and hepatic outcomes in a HFD-induced rat model. These results highlight Cers as early biomarkers of lipotoxic injury and CMD at earlier stages than traditional metabolic markers, positioning Sita as a promising agent for cardiometabolic therapy.

This study revealed distinct differences in how tested antidiabetic agents modulate Cer levels. HFD feeding significantly elevated CerC16:0 and CerC18:0 levels in serum, aligning with their established links to CMD,

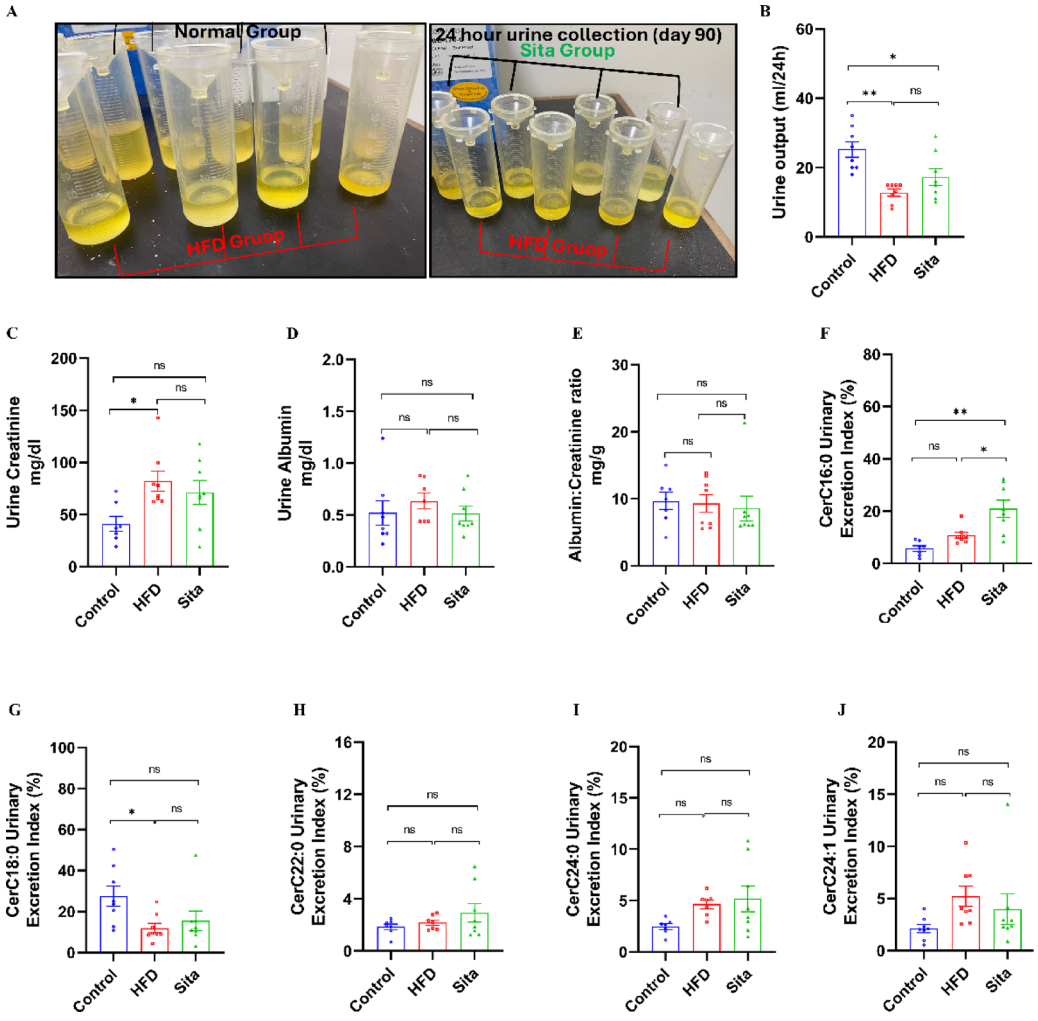

Fig. 4. Urine Output and urinary Cer indices during 24-hour urine collection. (**A**, **B**) Representative images of 24-hour urine collection from NC, HFD, and Sitagliptin-treated groups show a visual reduction in urine volume in the HFD group. Quantification of urine output (ml/24 h) indicates a significant decrease in the HFD group compared to Control, which is partially restored by Sitagliptin treatment. (**C**) Urine creatinine concentration. (**D**) Urine albumin concentration. (**E**) Urine albumin-to-creatinine ratio (UACR). (**F**-**J**) Urinary excretion indices (%) of CerC16:0, CerC18:0, CerC22:0, CerC24:0, and CerC24:1 on day 90, respectively. Data are presented as Mean ± SEM ($n = 8$ rats per group, biological replicates). Statistical significance was determined using one-way ANOVA followed by Tukey's post hoc test (B-G). $^{*}p < 0.05$, $^{**}p < 0.01$, ns = not significant.

including insulin resistance, endothelial dysfunction, and cardiovascular risk in animal and human studies[4,29]. While Lira and Saxa showed late or partial effects on the circulating levels of these high-risk Cer species, Sita consistently reduced both species in the serum as early as 14 days of treatment while sustaining these effects in the heart and liver tissues over the extended 90-day study. This differential efficacy likely stems from Sita's mechanism of action as a DPP-4 inhibitor, which enhances incretin signaling and lipid metabolism[22,30], and may indirectly influence Cer synthesis and clearance. Another proposed mechanism in which Sita may indirectly re-balance Cer metabolism is by improving insulin signaling and reducing lipid oversupply to the de novo Cer synthesis pathway. DPP-4 inhibition enhances incretin action and downstream AMPK activation, thereby limiting acetyl-CoA derived substrate flux into Cer biosynthesis[31,32]. In parallel, Sita has been reported to lower oxidative and inflammatory signals that activate sphingomyelinases, reducing the conversion of sphingomyelin to Cer[33,34]. Together, these mechanisms offer a plausible explanation for the observed decline in CerC16:0 and CerC18:0 and support the notion that modulation of Cer turnover contributes to Sita's cardiometabolic benefits. Although Lira demonstrated cardioprotective effects in other contexts[21,25], its impact on Cer metabolism in our study was less pronounced compared to Sita. Over the 35-day period, Lira did not significantly attenuate Cer accumulation, as levels of CerC16:0 and CerC18:0 continued to rise. This, also, aligns with findings from Akawi et al. where GLP-1 analogs like Lira showed variable effects on Cer species, with more pronounced modulation of circulating CerC16:0 requiring longer-term intervention[35]. The differential efficacy between Sita and Lira suggests that not all antidiabetic drugs target Cer metabolism equally, highlighting Sita's potential as a more direct modulator of Cer-driven metabolic dysfunction.

Intriguingly, while traditional metabolic markers (total cholesterol and fasting blood glucose) remained within normal ranges in Wistar rats for more than 12 weeks of HFD feeding, as previously reported[36], Cer concentrations showed divergence between groups as early as two weeks post-HFD initiation. Moreover, Cer profiles in serum, heart, and liver exhibited not only persistent but also significant alterations over time, surpassing even the subtle changes observed in the conventional metabolic markers. This suggests Cer's superior sensitivity as an early biomarker of metabolic dysregulation before overt metabolic abnormalities emerge.

Most strikingly, we observed tissue-specific patterns of Cer accumulation, with cardiac tissue showing particular vulnerability to CerC18:0 deposition. By Day 90, CerC18:0 levels in HFD-hearts reached 1.37 ± 0.103 nmol/g, exceeding all other measured species and even significantly higher than in the liver (0.364 ± 0.0141 nmol/g $p < 0.001$). This indicates the heart's unique susceptibility to CerC18:0 buildup under HFD conditions, which may contribute to the development of cardiac lipotoxicity, potentially linked to mitochondrial dysfunction, oxidative stress, and cardiomyocyte apoptosis, all of which are hallmarks of HFD-induced cardiac injury[16,37]. Our histopathological findings demonstrate two relevant phenomena: First, the time-dependent exacerbation of cardiac steatosis under chronic HFD exposure, with lipid accumulation increasing drastically between days 28 and 90. This progression paralleled the observed worsening of hepatic microvesicular steatosis (Fig. 3I), suggesting systemic lipotoxicity develops progressively despite stable traditional metabolic markers. Second, Sita's protective effects were maintained across both timepoints, reducing lipid droplet formation by comparable percentages despite the greater baseline severity at day 90. These histological changes strongly correlate with our biochemical data, specifically the elevation of CerC16:0 and CerC18:0, supporting the growing recognition that Cer-driven pathways contribute significantly to early lipotoxic organ injury in metabolic disease[11,38,39,40]. This aligns, as well, with recent evidence linking Cer to cardiomyocyte injury, as Haxhikadrija et al. (2025) showed similar Cer species accumulation (CerC16:0, C18:0, C22:0, C24:1) in iPSC-derived cardiomyocytes under ischemic stress, with associated mitochondrial dysfunction and apoptosis. Their α-MHC-CerS2 mouse model further confirmed these Cers induce cardiac apoptosis and fibrosis, mirroring our HFD-induced pathology[41].

At the molecular level, Sita treatment attenuated HFD-induced cardiac apoptosis (reduced Cleaved Caspase-3) and restored eNOS and phosphorylated AKT (pAKT) expression while preserving cTnT levels. These changes indicate a protective effect against cardiomyocyte damage and endothelial dysfunction, key hallmarks of CMD[5]. The upregulation of eNOS in the HFD group at day 90, coupled with reduced pAKT, may reflect a compensatory response to chronic oxidative stress and Cer accumulation, which Sita effectively counteracted. Similarly, the normalization of catalase expression suggests that Sita mitigates oxidative stress by enhancing antioxidant defenses, reinforcing its reported effects in diabetic and non-diabetic models[42,43]. Complementing its effects on Cers and oxidative stress, Sita treatment also attenuated the pro-inflammatory state, as evidenced by a trend toward reduced hepatic levels of IL-6 and TNF-α. This is mechanistically significant, as inflammatory cytokines have been reported as potent activators of sphingomyelinases[1,37,44], which convert sphingomyelin to Cer. Therefore, even a modest reduction in these inflammatory mediators likely contributes to the restoration of ceramide homeostasis and the observed improvement in hepatic steatosis under HFD conditions. These molecular insights provide a mechanistic basis for Sita's cardioprotective effects[45] and support the hypothesis that Cer dysregulation is a central driver of cardiometabolic pathology[4].

The urinary excretion indices of Cer provided insights into the role of Cer clearance in HFD-induced metabolic dysregulation. Remarkably, the urinary excretion index of CerC16:0 was significantly increased in the Sita-treated group compared to both the NC and HFD groups ($p < 0.01$ and $p < 0.05$, respectively), suggesting that Sita enhances the clearance of CerC16:0. This finding correlates with the observed reduction in serum CerC16:0 levels in the Sita group and may represent a different mechanism by which Sita modulates Cer metabolism. An effect could be a key part of Sita's mechanism in regulating Cer levels, possibly contributing to its cardioprotective effects. In contrast, CerC18:0 excretion was significantly reduced in the HFD group compared to the NC group ($p < 0.05$), despite a non-significant increase in the Sita group. This divergence advocates that Cer species may be differentially regulated via distinct metabolic or tissue-partitioning mechanisms, such as decreased synthesis, altered intracellular trafficking, or tissue sequestration[46]. Further studies will be needed to delineate these pathways. These findings highlight the complex interplay between Cer synthesis, metabolism, and excretion and suggest that enhancing Cer clearance may be a potential therapeutic strategy for managing CMD. It is noteworthy that alterations in urinary Cer profiles have been observed in human studies, where changes in urinary Cer levels reflected underlying metabolic and renal pathophysiology[47]. It is possible that the lack of significant clearance for other Cer types (e.g., CerC18:0, CerC22:0, CerC24:0, and CerC24:1) may require higher doses of Sita or more prolonged treatment durations to achieve similar effects. Sita's ability to normalize high-risk Cer species and their ratios (e.g., CerC16:0/24:0, CerC18:0/24:0, CerC24:1/24:0) along with ROS (H_2O_2 levels) suggests its dual role in mitigating lipid-induced toxicity and oxidative stress, potentially through enhanced Cer clearance, as evidenced by increased urinary CerC16:0 excretion. These findings align with previous reports that DPP4 inhibitors and GLP-1 agonists reduce oxidative stress and improve endothelial function[48,49], though our study uniquely positions Sita as a modulator of Cer homeostasis.

Conclusions

In conclusion, this study demonstrates that HFD correlates with Cer dysregulation across different tissues, with CerC18:0 playing a central role in cardiac and liver lipotoxicity. Sita treatment attenuates Cer accumulation, reduces oxidative stress, and ameliorates HFD-induced cardiac and hepatic steatosis. Nevertheless, its effects are more pronounced in specific tissues and Cer species. The pronounced accumulation of CerC18:0 in the heart highlights its potential as a therapeutic target for early lipotoxicity, while the tissue-specific responses to Sita emphasize the need for further research into the mechanisms of Cer metabolism. Importantly, the findings suggest that Cers may serve as reliable biomarkers for metabolic dysfunction, potentially even before traditional biomarkers such as cholesterol, triglycerides, and blood glucose levels are affected. This early detection capability

could provide a critical window for intervention, allowing for more timely and effective management of metabolic lipotoxicity. Future studies should explore the molecular pathways underlying Cer dysregulation as well as investigate the potential of combination therapies to enhance the therapeutic efficacy of Sita.

Limitation of the study

Although this study provides valuable insights into the modulation of Cer metabolism by Sita, several limitations should be acknowledged. First, the conclusions are restricted to an animal model, which may not fully replicate the complexity of human CMD pathology. Since the lipidomic analysis was limited to d18:1-based Cers, future studies should employ broader sphingolipidomic profiling, including other sphingoid base variants (e.g., d18:2 and d20:1) and Cer subclasses (e.g., dihydroCers, Cer-1-phosphates). Additionally, evaluating the key enzymes involved on Cer synthesis or degradation will be essential to fully elucidate the lipidomic signatures associated with lipotoxicity and their modulation by therapy. It is worth to mention that while the study establishes strong correlations between Sita treatment, reduced Cer levels and attenuation of cellular stress markers, it does not establish a causal relationship. Finally, the research findings suggest Cer to be early indicators of lipotoxic damage; however, confirmation of these results requires clinical studies for further validation in human populations.

Data availability

The data generated during and/or analysed during the current study are available from the corresponding author on reasonable request.

Received: 25 July 2025; Accepted: 28 November 2025
Published online: 14 December 2025

References

1. Shalaby, Y. M., Aidaros, A., Valappil, A., Ali, A., Akawi, N. & B. R. & Role of ceramides in the molecular pathogenesis and potential therapeutic strategies of cardiometabolic diseases: what we know so Far. *Front. cell. Dev. Biology*. **9**, 816301 (2022).
2. Field, B. C., Gordillo, R. & Scherer, P. E. The role of ceramides in diabetes and cardiovascular disease regulation of ceramides by adipokines. *Front. Endocrinol.* **11**, 569250 (2020).
3. Tkachev, A. I. et al. Ceramides: shared lipid biomarkers of cardiovascular disease and schizophrenia. *Consortium Psychiatricum*. **2**, 33–41 (2021).
4. Choi, R. H., Tatum, S. M., Symons, J. D., Summers, S. A. & Holland, W. L. Ceramides and other sphingolipids as drivers of cardiovascular disease. *Nat. Rev. Cardiol.* **18**, 701–711 (2021).
5. Zhang, D. X., Zou, A. P. & Li, P. L. Ceramide reduces endothelium-dependent vasodilation by increasing superoxide production in small bovine coronary arteries. *Circulat. Res.* **88**, 824–831 (2001).
6. Mantovani, A. & Dugo, C. Ceramides and risk of major adverse cardiovascular events: A meta-analysis of longitudinal studies. *J. Clin. Lipidol.* **14**, 176–185 (2020).
7. Vasile, V. C. et al. Ceramide scores predict cardiovascular risk in the community. *Arterioscler. Thromb. Vasc. Biol.* **41**, 1558–1569 (2021).
8. Meeusen, J. W. et al. Plasma ceramides: a novel predictor of major adverse cardiovascular events after coronary angiography. *Arterioscler. Thromb. Vasc. Biol.* **38**, 1933–1939 (2018).
9. Hilvo, M., Vasile, V. C., Donato, L. J., Hurme, R. & Laaksonen, R. Ceramides and ceramide scores: clinical applications for cardiometabolic risk stratification. *Front. Endocrinol.* **11**, 570628 (2020).
10. Akhiyat, N. et al. Plasma ceramide levels are elevated in patients with early coronary atherosclerosis and endothelial dysfunction. *J. Am. Heart Association*. **11**, e022852 (2022).
11. Liu, R. et al. Acid Sphingomyelinase promotes diabetic cardiomyopathy via NADPH oxidase 4 mediated apoptosis. *Cardiovasc. Diabetol.* **22**, 25 (2023).
12. Błachnio-Zabielska, A. U. et al. Cers1 but not CerS5 gene silencing, improves insulin sensitivity and glucose uptake in skeletal muscle. *Cells* **11**, 206 (2022).
13. Holland, W. L. Inhibition of ceramide synthesis ameliorates glucocorticoid-, saturated-fat-, and obesity-induced insulin resistance. *Cell Metabol.* **5**, 167–179 (2007).
14. Peterson, L. R. et al. Ceramide remodeling and risk of cardiovascular events and mortality. *J. Am. Heart Association*. **7**, e007931 (2018).
15. Simon, J. N. et al. Ceramide-mediated depression in cardiomyocyte contractility through PKC activation and modulation of myofilament protein phosphorylation. *Basic Res. Cardiol.* **109**, 1–15 (2014).
16. Turpin-Nolan, S. M. & Brüning, J. C. The role of ceramides in metabolic disorders: when size and localization matters. *Nat. Reviews Endocrinol.* **16**, 224–233 (2020).
17. Ho, Q. W. C., Zheng, X. & Ali, Y. Ceramide acyl chain length and its relevance to intracellular lipid regulation. *Int. J. Mol. Sci.* **23**, 9697 (2022).
18. Brown, E., Heerspink, H. J., Cuthbertson, D. J. & Wilding, J. P. SGLT2 inhibitors and GLP-1 receptor agonists: established and emerging indications. *J. Lancet*. **398**, 262–276 (2021).
19. Li, S. et al. SGLT-2 inhibitors or GLP-1 receptor agonists for adults with type 2 diabetes: a clinical practice guideline. *bmj* https://doi.org/10.1136/bmj.n1091 (2021).
20. Shalaby, Y. M. et al. Impact of sodium-glucose cotransporter-2 inhibitors on aging biomarkers and plasma ceramide levels in type 2 diabetes: beyond glycemic control. *Ann. Med.* **57**, 2496795 (2025).
21. El-Shafey, M. et al. Role of dapagliflozin and liraglutide on diabetes-induced cardiomyopathy in rats: implication of oxidative stress, inflammation, and apoptosis. *Front. Endocrinol.* **13**, 862394 (2022).
22. Sivalingam, S. et al. The effect of liraglutide and sitagliptin on oxidative stress in persons with type 2 diabetes. *Sci. Rep.* **11**, 10624 (2021).
23. Cessario, J., Pierre-Louis, V., Wahl, J. & Li, Z. Empagliflozin, alone or in combination with liraglutide, limits cell death in vitro: role of oxidative stress and nitric oxide. *Pharmacol. Rep.* **73**, 858–867 (2021).
24. Cao, Q. et al. Sitagliptin reduces endothelial dysfunction and apoptosis induced by high-fat diet and palmitate in thoracic aortas and endothelial cells via ROS-ER stress-CHOP pathway. *Front. Pharmacol.* **12**, 670389 (2021).
25. Cai, H., Zhou, L., Liu, J., Li, Z. & Chen, S. Independent and combined effects of liraglutide and aerobic interval training on glycemic control and cardiac protection in diabetic cardiomyopathy rats. *Biochem. Biophys. Res. Commun.* **629**, 112–120 (2022).
26. Vaghasiya, J., Sheth, N., Bhalodia, Y. & Manek, R. Sitagliptin protects renal ischemia reperfusion induced renal damage in diabetes. *Regul. Pept.* **166**, 48–54 (2011).

27. Nassar, N. N., Al-Shorbagy, M. Y., Arab, H. H. & Abdallah, D. M. Saxagliptin: a novel antiparkinsonian approach. *Neuropharmacology* **89**, 308–317 (2015).
28. Shalaby, Y. M. et al. Circulating ceramide levels and ratios in Emirati youth under 18 years: associations with cardiometabolic risk factors. *Lipids Health Dis.* **23**, 93 (2024).
29. Ren, L. et al. Abnormal plasma ceramides refine high-risk patients with worsening heart failure. *Front. Cardiovasc. Med.* **10**, 1185595 (2023).
30. Mulvihill, E. E. & Drucker, D. J. Pharmacology, physiology, and mechanisms of action of dipeptidyl peptidase-4 inhibitors. *Endocr. Rev.* **35**, 992–1019 (2014).
31. Zheng, W. et al. Dipeptidyl-peptidase 4 inhibitor sitagliptin ameliorates hepatic insulin resistance by modulating inflammation and autophagy in ob/ob mice. *Int. J. Endocrinol.* **2018**, 8309723 (2018).
32. Aroor, A. R. et al. Dipeptidyl peptidase-4 Inhibition ameliorates Western diet–induced hepatic steatosis and insulin resistance through hepatic lipid remodeling and modulation of hepatic mitochondrial function. *Diabetes* **64**, 1988–2001 (2015).
33. Wang, X. et al. Dipeptidyl peptidase-4 (DPP4) inhibitor sitagliptin alleviates liver inflammation of diabetic mice by acting as a ROS scavenger and inhibiting the NFκB pathway. *Cell. Death Discovery*. **7**, 236 (2021).
34. Sordillo, P. P., Sordillo, D. C. & Helson, L. The prolonged QT Interval: role of pro-inflammatory cytokines, reactive oxygen species and the ceramide and sphingosine-1 phosphate pathways. *in vivo* **29**, 619–636 (2015).
35. Akawi, N. et al. Fat-secreted ceramides regulate vascular redox state and influence outcomes in patients with cardiovascular disease. *J. Am. Coll. Cardiol.* **77**, 2494–2513 (2021).
36. Rocha, V. S. et al. High-fat diet-induced obesity model does not promote endothelial dysfunction via increasing Leptin/Akt/eNOS signaling. *Front. Physiol.* **10**, 268 (2019).
37. Chaurasia, B. & Summers, S. A. Ceramides in metabolism: key lipotoxic players. *Annu. Rev. Physiol.* **83**, 303–330 (2021).
38. Hajduch, E., Lachkar, F., Ferré, P. & Foufelle, F. Roles of ceramides in non-alcoholic fatty liver disease. *J. Clin. Med.* **10**, 792 (2021).
39. Jiang, M., Li, C., Liu, Q., Wang, A. & Lei, M. Inhibiting ceramide synthesis attenuates hepatic steatosis and fibrosis in rats with non-alcoholic fatty liver disease. *Front. Endocrinol.* **10**, 665 (2019).
40. Norheim, F. et al. Genetic, dietary, and sex-specific regulation of hepatic ceramides and the relationship between hepatic ceramides and IR [S]. *J. Lipid Res.* **59**, 1164–1174 (2018).
41. Haxhikadrija, P. et al. Inhibition of ceramide synthesis improves the outcome of ischemia/reperfusion injury in cardiomyocytes derived from human induced pluripotent stem cell. *Stem Cell Res. Ther.* **16**, 190 (2025).
42. Civantos, E. et al. Sitagliptin ameliorates oxidative stress in experimental diabetic nephropathy by diminishing the miR-200a/Keap-1/Nrf2 antioxidant pathway. *Diabetes metabolic syndrome obesity: targets therapy* **10**, 207–222 (2017).
43. Alam, M. A., Chowdhury, M. R. H., Jain, P., Sagor, M. A. T. & Reza, H. M. DPP-4 inhibitor sitagliptin prevents inflammation and oxidative stress of heart and kidney in two kidney and one clip (2K1C) rats. *Diabetol. Metab. Syndr.* **7**, 1–10 (2015).
44. De Mello, V. et al. Link between plasma ceramides, inflammation and insulin resistance: association with serum IL-6 concentration in patients with coronary heart disease. *Diabetologia* **52**, 2612–2615 (2009).
45. Chen, S. Y. et al. DPP4 as a potential candidate in cardiovascular disease. *Journal Inflamm. research* **15**, 5457–5469 (2022).
46. Hussain, M. M., Jin, W. & Jiang, X. C. Mechanisms involved in cellular ceramide homeostasis. *Nutr. Metabolism*. **9**, 71 (2012).
47. Morita, Y. et al. Alterations in urinary ceramides, sphingoid bases, and their phosphates among patients with kidney disease. *Front. Nephrol.* **4**, 1343181 (2024).
48. Avogaro, A. & Fadini, G. P. The effects of dipeptidyl peptidase-4 Inhibition on microvascular diabetes complications. *Diabetes Care*. **37**, 2884–2894 (2014).
49. Hullon, D. et al. The role of glucagon-like peptide-1 receptor (GLP-1R) agonists in enhancing endothelial function: a potential avenue for improving heart failure with preserved ejection fraction (HFpEF). *Cardiovasc. Diabetol.* **24**, 70 (2025).

Acknowledgements

The authors thank Professor Frank C. Howarth, Dr. Loay Lubbad and Dr. Sumaya Beegam for their valuable technical assistance and support during the animal experiments.

Author contributions

Y. S: Conceptualization, Experimental Work, Methodology, Investigation, Visualization, Formal Analysis, Writing – Original Draft.B. A: Investigation, Data Curation, Validation, Writing – Review & Editing.M. S: Tissue Processing and Staining.A.N: Investigation, Experimental Work, Methodology, Review & Editing.S. A: Histopathological Assessment, Figures Curation, Writing – Review & Editing.N. A: Conceptualization, Supervision, Funding Acquisition, Writing – Review & Editing, Project Administration.

Funding

The study was supported by a grant from the United Arab Emirates University (Fund no.: 12M106 [G00003664]).

Declarations

Competing interests

The authors declare no competing interests.

Additional information

Supplementary Information The online version contains supplementary material available at https://doi.org/10.1038/s41598-025-31001-5.

Correspondence and requests for materials should be addressed to N.A.